

# Depinning of three-dimensional drops from wettability defects

PH. BELTRAME<sup>1</sup>, P. HÄNGGI<sup>1</sup> and U. THIELE<sup>2</sup>

<sup>1</sup> *Institut für Physik, Universität Augsburg, D-86135 Augsburg, Germany*

<sup>2</sup> *Department of Mathematical Sciences, Loughborough University, Loughborough, Leicestershire, LE11 3TU, UK*

PACS 47.20.Ky – Nonlinearity, bifurcation, and symmetry breaking  
 PACS 47.55.D- – Drops and bubbles  
 PACS 68.08.-p – Liquid-solid interfaces

**Abstract.** - Substrate defects crucially influence the onset of sliding drop motion under lateral driving. A finite force is necessary to overcome the pinning influence even of microscale heterogeneities. The depinning dynamics of three-dimensional drops is studied for hydrophilic and hydrophobic wettability defects using a long-wave evolution equation for the film thickness profile. It is found that the nature of the depinning transition explains the experimentally observed stick-slip motion.

**Introduction.** – Drops sliding along a solid substrate under the influence of a lateral force are a very common physical phenomenon. The force might be gravity for drops on an inclined or vertical wall, centrifugal forces for drops on a rotating disk or external shear for drops in an ambient flow. Note that lateral gradients in wettability, temperature or electrical fields can as well drive sliding motion. For smooth homogeneous substrates an arbitrarily small driving force results in drops that move with constant velocity and shape [1–3]. Larger driving forces may lead to shape instabilities, e.g., trailing cusps may evolve that periodically emit small satellite drops [1, 4].

Real substrates, however, are normally not smooth. They are rough or have local chemical or topographical defects. Even microscopic defects can have a strong influence on the drop dynamics. The heterogeneities may cause stick-slip motion [5,6] or roughening [7,8] of moving contact lines, and are thought to be responsible for contact angle hysteresis [9–12]. Note that a local variation of the driving force (e.g., electrostatic field or temperature gradient) may play the same role as a substrate defect.

The present paper focuses on the depinning of three-dimensional drops from hydrophobic and hydrophilic line defects that pin them at their front and back, respectively: A hydrophobic defect is less wettable for the drop that therefore has to be forced to pass it. On the contrary, a hydrophilic defect is more wettable and the drop has to be forced to leave it as sketched in Fig. 1. A recent theoretical study of the depinning dynamics of less realistic two-dimensional drops employs lubrication approximation

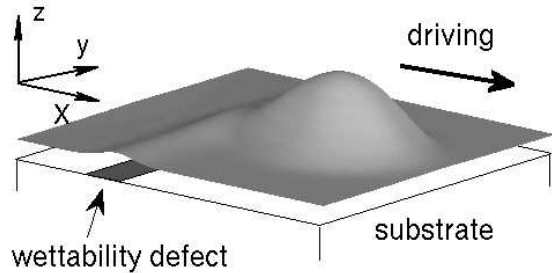


Fig. 1: Sketch of the three-dimensional geometry of the problem: a drop on a heterogeneous substrate and under a driving force  $\mu$  along the  $x$ -direction. Thereby the heterogeneous wettability is assumed to depend on the  $x$ -direction spatial direction only.

and finds stick-slip motion beyond depinning [13,14].

The present work is based on a thin film evolution equation in long-wave approximation [15,16] that incorporates wettability in the form of an additional pressure term – the so-called disjoining pressure [9]. It models the effective molecular interactions between the substrate and the free surface of the liquid, e.g., long-range apolar van der Waals interactions and short-range polar electrostatic or entropic interactions [17]. With the proper choice of terms such a disjoining pressure describes the behaviour of drops of partially wetting liquid with a small equilibrium contact angle that coexist with an ultra-thin precursor film. An

advantage of such a model is the absence of a contact line singularity. Note that although only small contact angles and small driving forces are compatible with the long-wave approximation results are often qualitatively correct for more general conditions. Incorporating wettability in the form of a disjoining pressure allows to study the influence of chemical substrate heterogeneities or defects by a spatial modulation of the involved material parameters. For dewetting thin films without lateral driving this is done in [18, 19].

The analysis of the two-dimensional problem in Refs. [13, 14] consists of a study of (i) steady drops and their stability based on continuation techniques for ordinary differential equations [20] and (ii) time-periodic solutions sliding over a regular array of defects based on 'standard' time-stepping schemes. The here presented study of the three-dimensional case is based on recently developed effective algorithms for both, the continuation of pinned steady drops described by a partial differential equation and the time simulation of the dynamics beyond depinning [21].

**Model and numerical method.** – We consider a liquid layer or drop on an inhomogeneous two-dimensional solid substrate as sketched in Fig. 1. The liquid partially wets the substrate (with a small equilibrium contact angle) and is subject to a small constant lateral force  $\mu$  that acts in the  $x$ -direction. Employing the long-wave or lubrication approximation the dimensionless evolution equation for the film thickness profile  $h(x, y, t)$  is derived from the Navier-Stokes equations, continuity and boundary conditions (no-slip at substrate, force equilibria at free surface) [13, 15, 16]. It reads

$$\partial_t h = -\nabla \cdot \{m(h) [\nabla (\Delta h + \Pi(h, x)) + \mu \mathbf{e}_x]\}, \quad (1)$$

where  $\nabla = (\partial_x, \partial_y)$  and  $\Delta = \partial_{xx}^2 + \partial_{yy}^2$  are the planar gradient and Laplace operator, respectively. The mobility function  $m(h) = h^3$  corresponds to Poiseuille flow and  $\Delta h$  represents the Laplace pressure (capillarity). The disjoining pressure  $\Pi(h, x)$  models the position-dependent wetting properties that in the case of transverse line defects only depend on the streamwise direction. The literature discusses a plethora of different functional forms for  $\Pi(h)$  [9, 22]. Most model the presence of an ultra-thin precursor film of about 1-10 nm thickness and thereby avoid a 'true' film rupture. We employ long-range apolar van der Waals interactions combined with a short-range polar interaction [9, 17, 23]

$$\Pi(h, x) = \frac{b}{h^3} - (1 + \epsilon \xi(x)) e^{-h}, \quad (2)$$

where  $\epsilon$  and  $\xi(x)$  are the amplitude and profile of the heterogeneity, respectively. To model a localized defect  $\xi(x)$  is based on Jacobi elliptic functions as described in [13, 14]. Typical examples can be seen below in Fig. 2. The amplitude  $\epsilon$  represents the wettability contrast. For  $\epsilon < 0$  [ $\epsilon > 0$ ]

the defect is less [more] wettable than the surrounding substrate, i.e., the defect is hydrophobic [hydrophilic]. Based on the Jacobi functions we study drops on a periodic array of defects. The period  $L_x$  is chosen sufficiently large to avoid interactions between subsequent drops/defects. The imposed spatial periodicity allows to characterize stick-slip motion by its period in time.

Based on Eq. (1) with (2) the depinning behaviour in the three-dimensional (3d) case is analysed following the methodology used in [13, 14] for the two-dimensional (2d) case. Steady-state solutions (pinned drops) and their stability are determined using continuation techniques and the stick-slip motion beyond the depinning threshold is analysed using time-stepping algorithms. In the 2d case an explicit scheme suffices for the latter. The continuation can be performed using the package AUTO [24] as the underlying equation corresponds to a system of ODE's [16]. In the 3d case an effective and exact time simulation of Eq. (1) is challenging and leads to a number of numerical problems [4, 25, 26]. Here we employ a recently developed approach [21] based on exponential propagation [27]. It allows for a very good estimate of the optimal timestep for the different regimes of the dynamics. This is of paramount importance as close to the depinning transition it needs to be varied over many orders of magnitude. The second advantage lies in the possibility to adapt the time-stepping scheme in a way that it can be used to continue the branches of steady drop states and to determine their stability. For details see Ref. [21].

**Depinning of 2d drops.** – Before focusing on the 3d case we shortly present results for 2d using equivalent parameter values to allow for a qualitative and quantitative comparison. Without lateral force ( $\mu = 0$ ) there exists a unique stable drop solution for each wettability contrast  $\epsilon$ . The drop sits on top of a hydrophilic defect (dashed line in Fig. 2(a)) or in the middle between hydrophobic defects (dashed line in Fig. 2(b)). Note that other steady solutions may exist that are normally unstable. For an in-depth study of solutions on a horizontal substrate (for another  $\Pi(h)$ ) see [19].

Increasing the lateral driving force  $\mu$  from zero the drop does not start to slide as for the homogeneous substrate, but remains pinned by the defect. A hydrophobic defect blocks the drop at the front, it becomes compressed and heightens (see Fig. 2(b)) until it finally depins. This can best be seen in the bifurcation diagram Fig. 2(d) where the norm of stable and unstable steady solutions is shown in dependence of  $\mu$  for several wettability contrasts. The norm of the stable drop solution first increases, then decreases slightly and the branch annihilates with an unstable one at  $\mu_c$ . In contrast, a hydrophilic defect holds a drop at its back, with increasing driving it becomes stretched and lower (see Fig. 2(a)) until it finally depins. The accompanying bifurcation diagram (Fig. 2(c)) shows that the norm decreases till the branch annihilates with an unstable one, e.g., for  $\epsilon = -0.3$  at  $\mu_c \approx 0.005$ .

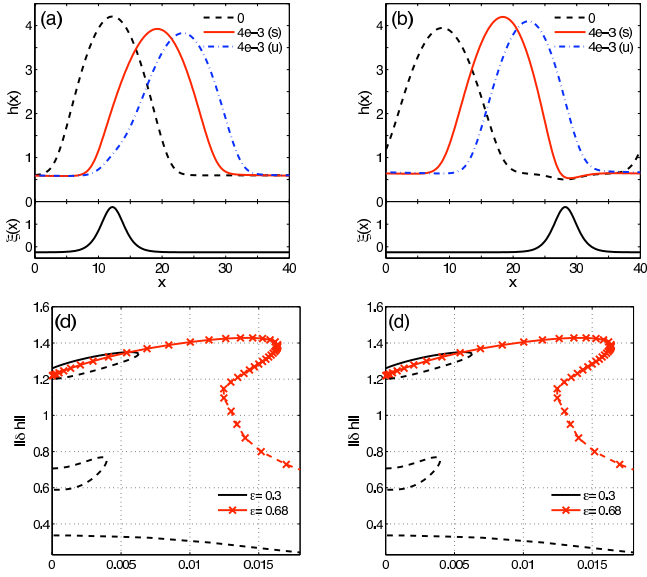


Fig. 2: Selected drop profiles (top row) and corresponding bifurcation diagrams (bottom row) for localized hydrophilic ( $\epsilon = 0.3$ , left column) and hydrophobic ( $\epsilon = -0.3$ , right column) defect in the 2d case. (a) and (b) give steady drop profiles for several driving forces  $\mu \geq 0$  as given in the legend. For  $\mu = 4 \cdot 10^{-3}$  stable (solid line with symbol “s”) and unstable (dotted line with symbol “u”) steady drops are represented. The lower part of the panels gives the heterogeneity profile  $\xi(x)$ . (c) and (d) characterize branches of steady drop solutions by the dependence of their  $L^2$  norm ( $\|\delta h\| = \sqrt{\int_0^L (h - \bar{h})^2 dx/L}$ ) on the lateral driving force  $\mu$  for various defect strength  $\epsilon$  as given in the legend. Dashed lines indicate unstable solutions. Domain length, volume and resulting drop height on a homogeneous substrate are  $L_x = 40$ ,  $V = 66$  and  $h_{max} = 4.0$ , respectively.

Beyond the critical value  $\mu_c$ , there exists in both cases only a single branch of steady solutions that are all linearly unstable. Its norm approaches zero with increasing  $\mu$  (not shown) indicating that it corresponds to slightly modulated film solutions. This state being unstable, a time-dependent state is expected that corresponds to sliding drops. In the 2d case such solutions were discussed in Ref. [13]. Related solutions and the character of the depinning transition for the 3d case will be discussed next.

**Depinning of 3d drops.** – We consider now the full 3d geometry as sketched in Fig. 1. In particular, we look at hydrophilic and hydrophobic line defects that lie orthogonal to the direction of the driving force. In the present 3d setting one can re-interpret the findings for 2d drops as referring to the depinning of a liquid ridge from a line defect assuming that the transverse translational symmetry is not broken in the depinning process.

To compare the depinning of such a ridge and the one of a true 3d drop we use the continuation and time-stepping techniques outlined above. Furthermore all parameters with the exception of the drop volume are chosen as in

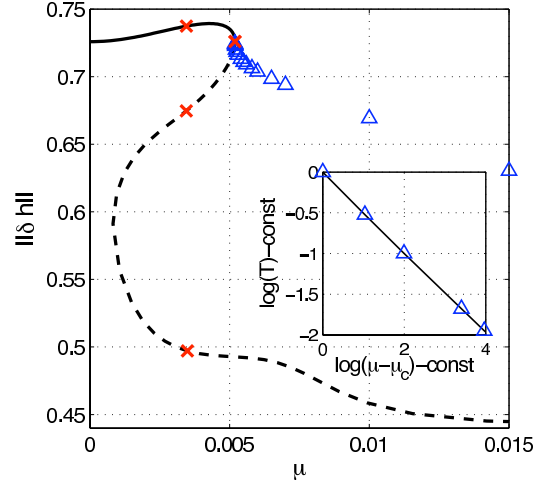


Fig. 3: Bifurcation diagram for drops pinned by a hydrophilic line defect of strength  $\epsilon = -0.3$ . Shown is the  $L^2$  norm  $\|\delta h\|$  of steady solutions in dependence of the lateral driving force  $\mu$ . The branch of stable pinned drops corresponds to the solid line whereas unstable solutions are given as dotted lines. Beyond the depinning bifurcation, triangles represent the time-averaged  $L^2$  norm of time-periodic solutions that correspond to sliding drops performing a stick-slip motion. The domain size is  $40 \times 40$ . Crosses indicate profiles given in Fig. 4. The inset gives for the stick-slip motion the dependence of the time-period on  $\mu - \mu_c$ . The straight line corresponds to a power law with exponent  $-1/2$ .

the 2d case. For the latter we use a value such that the maximal drop height on a homogeneous substrate without driving force ( $\mu = 0$ ) is equal to the one of the ridge.

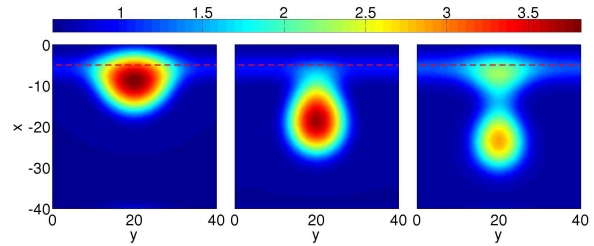


Fig. 4: Shown are contours of steady drop solutions for a hydrophilic defect for  $\mu = 3.5 \cdot 10^{-3}$ . Profiles from left to right correspond to crosses in Fig. 3 from high to low norm. The left panel presents the stable pinned drop. The thin horizontal line marks the wettability maximum. The remaining parameters are as in Fig. 3.

Fig. 3 shows the bifurcation diagram for a single drop on a square domain. The stable drop is pinned at its back by the hydrophilic line defect with  $\epsilon = -0.3$ . On the horizontal substrate ( $\mu = 0$ ) the drop sits symmetrically on the defect its contour being an ellipse with the long axis on the defect (not shown). When increasing  $\mu$  the drop moves to the downstream side of the defect where it is retained by the high wettability patch below its tail. With increasing  $\mu$  it stretches downstream but is compressed transversally.

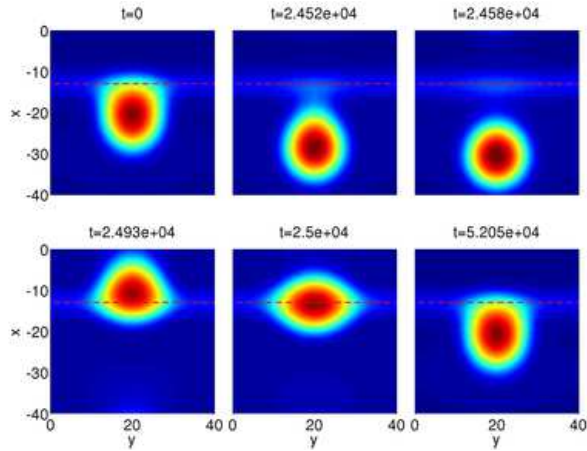


Fig. 5: Shown are snapshots of drop profiles at different stages of a stick-slip cycle (at times given below the individual panels) for a drop depinning from a hydrophilic line defect (marked by the horizontal line). The chosen driving  $\mu = 5.193 \cdot 10^{-3}$  is still close to the critical  $\mu_c$ . Color code and remaining parameters are as in 3.

The combined effect of the two processes leads contrary to the 2d case to an increase of the norm. The stable branch loses its stability via a saddle-node bifurcation at the critical driving  $\mu_c = 5.193 \cdot 10^{-3}$ . The continuing unstable branch is turned towards smaller  $\mu$ . It turns back again at a further saddle-node bifurcation and the resulting 'low-norm' branch then continues towards large  $\mu$ . A selection of steady stable and unstable drop solutions corresponding to the crosses in Fig. 3 is given in Fig. 4. The left panel corresponds to the pinned stable drop described above, the middle panel represents an unstable drop that one could call "at depinning": it has an oval front shape and is connected to the hydrophilic patch by a thin bridge that almost looks cusp-like and seems to be at the point of breaking. Physically it corresponds to a threshold solution: If it is moved a bit upstream [downstream] it retracts [slips to the next defect] and converges to the stable drop solution. The left panel, finally, gives the unstable solution of lowest norm. It resembles two drops joined by a thin thread with the smaller one sitting on the heterogeneity. The character of solutions on this branch at large  $\mu$  is discussed below.

For  $\mu > \mu_c$  no steady stable solutions exist and we expect the system to exhibit a time-dependent behaviour. In particular, we expect in the present spatially periodic setting that drops depin from one hydrophilic defect and slide to the next one. There they do not stop but only slow down as the defect tries to retain them. We probe this behaviour using a time-stepping algorithm. The time-averaged norm for several  $\mu$  is given in Fig. 3 and one can well appreciate that the corresponding solution branch emerges from the saddle-node bifurcation at  $\mu_c$  indicating that it is actually a Saddle Node Infinite PERiod (SNIPER) bifurcation. This is furthermore corroborated

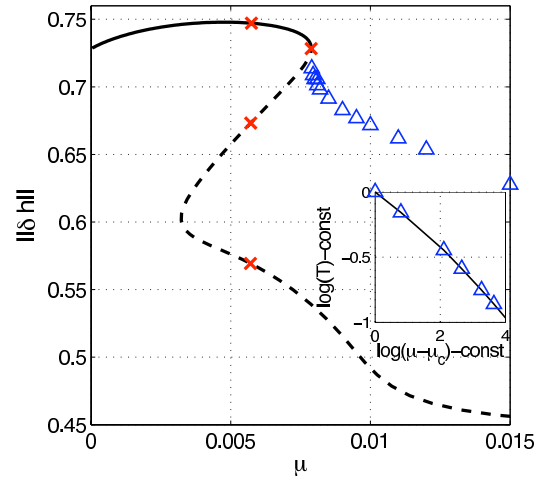


Fig. 6: Bifurcation diagram for drops pinned by a hydrophobic line defect of strength  $\epsilon = 0.3$ . The presented norms, line styles, symbols, domain size and inset are as in Fig. 3. Corresponding profiles are given in Fig. 7. The straight line in the inset corresponds to a power law with exponent  $-1/4$ .

by the square root dependence of the inverse time-period (mean sliding speed) on  $\mu - \mu_c$  that is given in the inset of Fig. 3 [13,28]. An example of a time series of snapshots for a stick-slip motion of a single drop is given in Fig. 5. Note that the times at which the snapshots are taken are not equidistant. It takes the drop about 25000 time units to slowly stretch away from the defect (snapshot 1 to 2). Then within 500 units it depins and slides to the next defect (snapshot 2 to 5), where it needs another 25000 units to reach an identical state as in snapshot 1 (snapshot 5 to 6). The depinning itself resembles a pinch-off event at a water tap: the bridge between drop and a 'reservoir' on the hydrophilic stripe becomes thinner until it snaps. Once the main drop slides a small drop remains behind on the defect. All together for the chosen value of  $\mu$  the ratio of stick/stretch and slip phase is about 50 : 1. The ratio diverges when approaching the bifurcation.

Next we discuss the case of a hydrophobic defect. Fig. 6 is the corresponding bifurcation diagram. It shows as solid line stable solutions corresponding to single drops blocked at their front by the line defect with  $\epsilon = 0.3$ . Dashed lines indicate unstable steady solutions. The general behaviour resembles strongly the related 2d case and as well the hydrophilic case. In particular, does the norm of the stable solutions increase with increasing  $\mu$  as the drop is increasingly pushed against the defect and becomes therefore steeper. The drop itself becomes more oval as its transverse width increases but the streamwise one decreases. An example of such a stable steady drop can be seen in the left panel of Fig. 7. The two other panels represent the two unstable solutions that exist for identical  $\mu$  (crosses in Fig. 6). Both unstable drops are situated mainly upstream of the defect but have downstream protrusions of different length and strength that reach the substrate beyond the

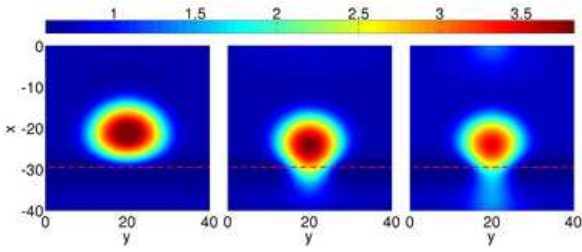


Fig. 7: Shown are contours of steady drop solutions for a hydrophobic defect for  $\mu = 5.7 \cdot 10^{-3}$ . Profiles from left to right correspond to crosses in Fig. 6 from high to low norm. The left panel presents the stable pinned drop. The horizontal line marks the wettability minimum. The remaining parameters are as in Fig. 6.

defect. The drop on the middle branch corresponds to a threshold solution as in the hydrophilic case.

Time simulations indicate that depinning occurs again via a sniper bifurcation, i.e., a branch of time-periodic solutions emerges from the saddle-node at  $\mu_c$ . However, the time-period does not diverge as  $(\mu - \mu_c)^{-1/2}$  but rather with the power  $-1/4$  (inset of Fig. 6). An example of a time series of snapshots for a stick-slip motion of a depinned drop is given in Fig. 8. The drop needs about 1600 time units to slowly let a ‘protrusion’ creep over the defect (snapshot 1 to 2). Then within 400 units it depins and slides to the next defect (snapshot 2 to 5), where it needs another 1200 units to reach the state as in snapshot 1 (snapshot 5 to 6). Then the cycle starts again. All together for the chosen value of  $\mu$  the ratio of stick and slip phase is about 7 : 1. Once the drop is depinned a small drop is retained behind the defect (snapshot 4).

Comparing the 2d and 3d cases we find that the depinning behaviour for drops of equal height agrees qualitatively, but quantitatively there is a small systematic difference. In both cases we find depinning transitions via a sniper bifurcation at a critical driving  $\mu_c$ . However, in 3d  $\mu_c$  is about 10-15% larger than the one in 2d. This is a result of the smaller mass per lateral length the 3d drop has as compared to the ridge. Such an effect increases  $\mu_c$  as it implies a smaller ‘effective 2d loading’ in the 3d case. Actually, from the dependency on loading in 2d (see [13]) one would expect an even larger difference. The reason for the small increase may be the additional degree of freedom that a true 3d drop has as compared to a translationally invariant ridge. It allows the drop to ‘probe’ the barrier locally by an advancing protrusion (in the hydrophobic case) or by thinning its backward bridge to the defect (in the hydrophilic case). It can therefore use a pathway of morphological changes for depinning that a 2d drop is not able to use. Note that individual stations of this pathway that can be seen in Figs. 5 and 8 do very much resemble the unstable steady solutions presented in Figs. 4 and 7, respectively. This indicates that the steady solutions that exist below  $\mu_c$  are still present in the phase space as ‘ghost solutions’ [28] and can be seen in the course of the time

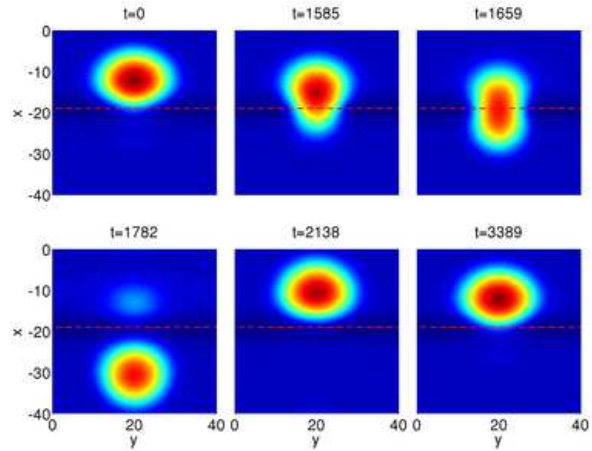


Fig. 8: Shown are snapshots of drop profiles at different stages of a stick-slip cycle for a depinned drop near the depinning bifurcation (at  $\mu = 7.898 \cdot 10^{-3}$  and times as given below the individual panels) for a hydrophobic line defect (marked by the horizontal line). Color code and remaining parameters are as in 6.

periodic motion beyond  $\mu_c$ . When we have discussed that the depinning behaviour for  $\epsilon = \pm 0.3$  in 2d and 3d is very similar we have focused on the branch of pinned drops only. Note that the connectivity of the unstable branches is not that similar. In this respect the 3d case resembles the 2d case at a larger contrast  $\epsilon$ .

Finally, we discuss the character of the single remaining steady state solution for large  $\mu$ . Comparing bifurcation diagrams for large increasing  $\mu$  (not shown) one notes that in the 2d case the norm approaches zero and the solutions resemble slightly modulated films. In contrast, in 3d the norm approaches a finite value, i.e., there remains a non-trivial large amplitude structure. The character of this structure can be appreciated in Fig. 9. Equally for hydrophilic as for hydrophobic defects one finds a rivulet with drop-like transverse cross sections and comparatively small variation in streamwise direction. Increasing  $\mu$  the streamwise modulation becomes even smaller and the thickness profiles in the transverse direction are very close to steady 2d drops on horizontal substrates of corresponding wettability. The rivulet is linearly unstable below a large finite driving  $\mu_r$ . There it stabilizes via a Hopf bifurcation that as well forms the end point of the branch of time-periodic solutions.

**Conclusion.** – We have studied depinning three-dimensional drops under lateral driving for localized hydrophobic and hydrophilic line defects employing on the one hand continuation techniques to obtain steady-state solutions (pinned drops and rivulets) and their stability and on the other hand a time-stepping algorithm to study the dynamics of the stick-slip motion beyond depinning. We have found that for the studied parameter range the depinning behavior is qualitatively similar in 2d and 3d: Drops are pinned up to a critical driving  $\mu_c$  where they

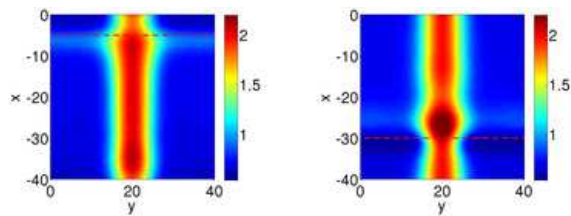


Fig. 9: Shown are contours of steady rivulet solutions for large driving force  $\mu = 0.05$  for (a) hydrophilic and (b) hydrophobic line defects. The remaining parameters are as in Figs. 3, and 6, respectively. The horizontal line marks the extrema of the wettability profile.

depin via a sniper bifurcation. Quantitatively there exists a small systematic difference – the 3d  $\mu_c$  is slightly larger than the 2d one. Our interpretation is that the difference results mainly from a lower “effective 2d loading” in the 3d case but it has as well to be taken into account that the 3d drop has additional degree of freedom enabling it to employ pathways of morphological changes for depinning that a 2d drop is not able to access.

The sniper bifurcation is in the hydrophilic case characterized by a square-root power law dependence of the inverse time scale of depinning on the distance from threshold  $\mu - \mu_c$ . Beyond  $\mu_c$  the unsteady motion resembles the stick-slip motion observed in experiment: The advance of the drop is extremely slow when it ‘creeps away’ from the hydrophilic region, and very fast once the thread connecting the back of the drop to the defect has broken and the drop slides to the next defect. The difference in time scales for the stick and the slip phase diverges when approaching  $\mu_c$ . For a hydrophilic defect, however, we have found a degenerate sniper bifurcation as the power law has an exponent of about 1/4. Re-considering the 2d case we found that there as well in the hydrophobic case the power is about 1/3, i.e., it differs from the expected 1/2 (cf. [13]). This may result from a degeneracy of the problem that has, however, still to be identified.

Note that for hydrophobic defects of large strength depinning may occur at very large driving via a Hopf instead of a sniper bifurcation [14]. Then depinning is caused by the flow in the wetting layer. For realistic forces the effect can not be observed for partially wetting nano- or micro-drops on an incline or rotating disc and we have not considered the parameter regime here. Note, however, that micro-drops of dielectric liquids generated by an electric field in a capacitor can coexist with a thick wetting layer of 100nm to 1 $\mu$ m stabilized by van der Waals interaction [29,30]. In such a setting both depinning mechanisms should be observable using gravity as the driving force (see appendix of [13]).

\*\*\*

We acknowledge support by the EU [MRTN-CT-2004005728 PATTERNS] and the DFG [SFB 486, B13].

## REFERENCES

- [1] PODGORSKI T., FLESSELLES J.-M. and LIMAT L., *Phys. Rev. Lett.* , **87** (2001) 036102.
- [2] THIELE U., VELARDE M. G., NEUFFER K., BESTEHORN M. and POMEAU Y., *Phys. Rev. E* , **64** (2001) 061601.
- [3] SNOEIJER J. H., LE GRAND N., LIMAT L., STONE H. A. and EGGERS J., *Phys. Fluids* , **19** (2007) 042104.
- [4] THIELE U., NEUFFER K., BESTEHORN M., POMEAU Y. and VELARDE M. G., *Colloid Surf. A* , **206** (2002) 87.
- [5] SCHÄFFER E. and WONG P. Z., *Phys. Rev. Lett.* , **80** (1998) 3069.
- [6] TAVANA H., YANG G. C., YIP C. M., APPELHANS D., ZSCHOCHÉ S., GRUNDKE K., HAIR M. L. and NEUMANN A. W., *Langmuir* , **22** (2006) 628–36.
- [7] GOLESTANIAN R. and RAPHAËL E., *Europhys. Lett.* , **55** (2001) 228.
- [8] ROBBINS M. O. and JOANNY J. F., *Europhys. Lett.* , **3** (1987) 729.
- [9] DE GENNES P.-G., *Rev. Mod. Phys.* , **57** (1985) 827.
- [10] LEGER L. and JOANNY J. F., *Rep. Prog. Phys.* , **55** (1992) 431.
- [11] QUÉRÉ D., AZZOPARDI M. J. and DELATTRE L., *Langmuir* , **14** (1998) 2213.
- [12] SPELT P. D. M., *J. Fluid Mech.* , **561** (2006) 439.
- [13] THIELE U. and KNOBLOCH E., *New J. Phys.* , **8** (2006) 313, 1.
- [14] THIELE U. and KNOBLOCH E., *Phys. Rev. Lett.* , **97** (2006) 204501.
- [15] ORON A., DAVIS S. H. and BANKOFF S. G., *Rev. Mod. Phys.* , **69** (1997) 931.
- [16] KALLIADASIS S. and THIELE U., (Editors) *Thin Films of Soft Matter* (Springer, Wien / New York) 2007 CISM 490.
- [17] SHARMA A., *Langmuir* , **9** (1993) 861.
- [18] KONNUR R., KARGUPTA K. and SHARMA A., *Phys. Rev. Lett.* , **84** (2000) 931.
- [19] THIELE U., BRUSCH L., BESTEHORN M. and BÄR M., *Eur. Phys. J. E* , **11** (2003) 255.
- [20] DOEDEL E., KELLER H. B. and KERNEVEZ J. P., *Int. J. Bifurcation Chaos* , **1** (1991) 493.
- [21] BELTRAME P. and THIELE U., *submitted* , (2008) .
- [22] TELETZKE G. F., DAVIS H. T. and SCRIVEN L. E., *Rev. Phys. Appl.* , **23** (1988) 989.
- [23] THIELE U., VELARDE M. G. and NEUFFER K., *Phys. Rev. Lett.* , **87** (2001) 016104.
- [24] DOEDEL E., PAFFENROTH R., CHAMPNEYS A., FAIRGRIEVE T., KUZNETSOV Y., SANDSTEDTE B. and WANG X., Tech. Rep. Caltech (2001).
- [25] BERTOZZI A. L., GRÜN G. and WITELSKI T. P., *Nonlinearity* , **14** (2001) 1569.
- [26] BECKER J. and GRÜN G., *J. Phys.: Condens. Matter* , **17** (2005) S291.
- [27] FRIESNER R. A., TUCKERMAN L. S., DORNBLASER B. C. and RUSSO T. V., *J. Sci. Comp.* , **4** (1989) 327.
- [28] STROGATZ S. H., *Nonlinear Dynamics and Chaos* (Addison-Wesley) 1994.
- [29] LIN Z., KERLE T., BAKER S. M., HOAGLAND D. A., SCHÄFFER E., STEINER U. and RUSSELL T. P., *J. Chem. Phys.* , **114** (2001) 2377.
- [30] MERKT D., POTOTSKY A., BESTEHORN M. and THIELE U., *Phys. Fluids* , **17** (2005) 064104.